Layer Detection in Radar Sounder Images

Andrew Hilger
Electrical Engineering
amhilger@stanford.edu

Sarah Hooper
Electrical Engineering
smhooper@stanford.edu

Cedric Yue Sik Kin
Electrical Engineering
cedyue@stanford.edu

Abstract

Radar investigations of glaciers rely on accurate identification of layer features in radar survey images (radargrams). Traditionally, these features have been identified ("picked") manually or semi-manually. To improve the efficiency and consistency of this picking process, we present an automated method to identify the glacier surface and glacier-bedrock interface in radargrams. This method identified 99.9% of surface layer points and 84% of bed layer points within within 20 pixels of accuracy.

1. Background

In an era of higher temperatures and thinning ice sheets, understanding Earth's polar regions is increasingly important. To better predict the response of sea levels to this change, many scientists have modeled glacier responses. However, these models are poorly constrained because of limited understanding of boundary conditions at the bedrock of the glacier. The glacier's basal properties (e.g., frozen bedrock, loose glacial till, thawed water) significantly impacts that glaciers movement. For example, a glacier on thawed water will slide over the bed layer, while ocean water penetration will lubricate the glacier's movement.

To better understand subglacial conditions, researchers have conducted thousands of kilometers of radar surveys [3]. These surveys use synthetic aperture radar (SAR) processing techniques to combine a sequence of radar returns into a cross-section of the glacier along the survey track. An example of such a radargram is shown in Figure 1.

Although these surveys have succeeded in mapping subglacial topography, much work remains in understanding englacial processes and subglacial conditions. One prerequisite for analyzing radar surveys is identifying features such as the glacier surface, bed, and englacial layers from the radargrams. However, identifying these features (often referred to as picking) is time consuming and can require hundreds of person hours, even with layer tracing GUIs designed specifically to facilitate this task.

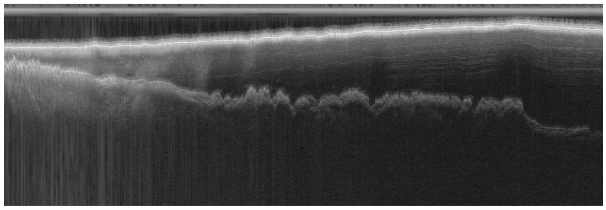

Figure 1. Cropped focused radargram of West Antarctica's Amundsen Sea Embayment [3].

Previous work includes [1], which uses a horizontally extended Prewitt operator to accentuate englacial layers. However, the technique makes no provision for layers of having returns of varying widths and powers. [5] describes a wavelet transform to accentuate layers of varying widths, as well as using a Hough transform for tracing layers. However, the Hough-transform method assumes slowly varying layer slope, which is true for englacial layers but not for the bed layer, which has sharp changes in layer slope due to topography. [4] describes orientation-specific edge detection and layer tracing techniques using rotated Gaussian filters. This method also assumes parallel layers, and uses a computationally intensive exhaustive search over layer slopes to trace layers. Thus, [1], [5], and [4] are better suited to identifying englacial layers than the bed layer.

In this project, we combine and adapt methods from the foregoing sources to identify the bed layer while maintaining reasonable computational time.

2. Methods

Our layer detection pipeline consists of three stages. First, we apply an edge-enhancement filter to intensify the surface and bed. Using this edge-enhanced image, we then select seed points by identifying maximum intensity values along the range direction. Finally, we use the seed points to guide layer-tracing. For each stage, we investigated different approaches and quantified each approach's ability to identify the surface and bed layers.

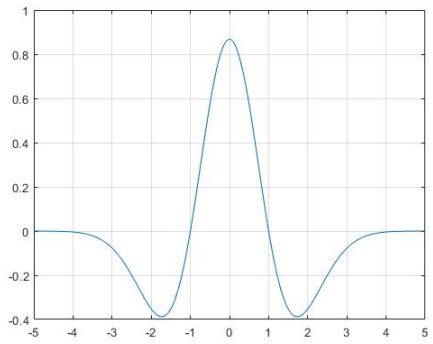

Figure 2. The Ricker wavelet has an effective support between $[-5a, 5a]$, where a is the wavelet scale parameter.

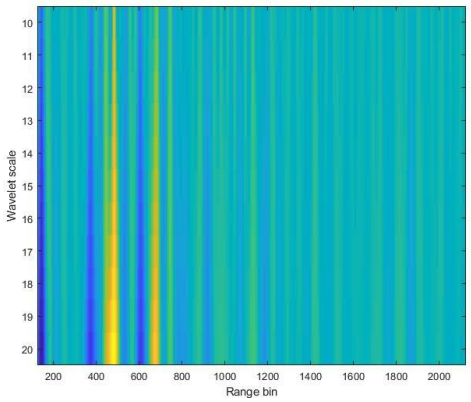

Figure 3. Wavelet transform of one range column, with wavelet scale a on the vertical axis and range bin number on the horizontal axis. Color scale shows more positive response in yellow, more negative response in blue, medium response in green.

2.1. Edge enhancement

We initially explored gradient-based edge detection filters such as the Prewitt, Sobel, and Roberts filters. However, these detectors had mediocre results for this application. Accordingly, we implemented edge enhancement using a sharpening filter, a 1-d Ricker wavelet transform, a directional Gaussian filter, and a tophat filter to improve results.

2.1.1 Sharpening filter

First, the image was sharpened in order to improve subsequent edge detection. To sharpen the image, we took the difference between the original image and the image after being filtered with a 2-d Gaussian filter. Applying a sharpening filter before the wavelet transform improved our layer-identification success rate.

2.1.2 Ricker wavelet transform

The Ricker wavelet takes the form $\psi = \frac{2}{\pi^{\frac{1}{4}}\sqrt{3*a}} * (1 - (\frac{t}{a})^2) * e^{-\frac{t^2}{2a^2}}$, where a is the scaling parameter and t is the input domain. Figure 2 illustrates a Ricker wavelet with a scale a = 1. Convolving the 1-d Ricker wavelet ψ with a range return (one column of the radargram) effectively performs horizontal edge detection. This is because the Ricker wavelet (which can be approximated by a difference of Gaussians) is effectively a band-pass filter for medium-frequency components.

The filter accentuates peaks and flattens monotonic slopes. The filter has the greatest response to a peak when the scale parameter of the peak a matches the peak's width. The surface layer has a consistent peak width because it is a consistent distance from the radar and doesn't experience any englacial losses. In contrast, the bed layer's power varies significantly depending on depth. The bed layer's width is proportional to depth, but also depends on the bed's roughness and whether other structures (e.g., accretion plumes) are present between the bedrock and the ice. Thus, it is beneficial to use a variety of scales to detect the bed. Figure 3 demonstrates the response of a single range line to the wavelet transform performed at a range of scales between $a = 10$ and $a = 20$. A variety of scale ranges were tested. The foregoing range was used because it preferentially enhanced the surface and bed layers relative to englacial layers. This is because englacial layers have narrower peaks than the bed and surface layers, so excluding scales $a < 10$ attenuates the englacial layers' response. Other wavelets such as the real-valued Morlet are discussed in [5], but the authors find that the Ricker wavelet performs best for identifying peaks corresponding to layers.

An example output from the Ricker wavelet filtering process is shown in Figure 3. The strong response on the left corresponds to the surface layer, and the strong response immediately to the right corresponds to the bed layer. To produce a column of the transformed image, the responses are summed across scale space. This process is then repeated for each column, thereby producing the edge enhanced image in Figure 4.

2.1.3 Directional Gaussian filters

[4] describes using directional Guassian filters for edge detection. In this approach, we applied a 2d Gaussian filter with $\sigma_x > \sigma_y$ to the image and stored the result. The Gaussian filter was then rotated five degrees and once again applied to the image. This process was repeated until the filter had rotated a full 360° and each filtered image was stored.

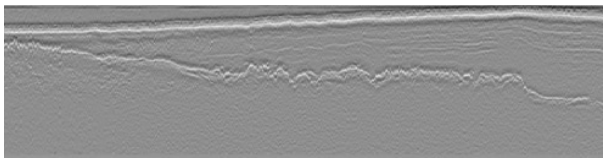

Figure 4. Sum of images produced by filtering sharpened radargram with many scales of Ricker wavelets.

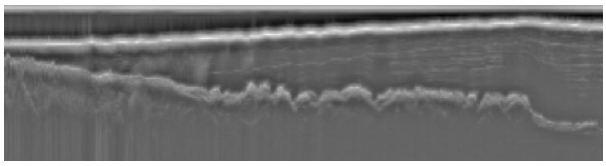

Figure 5. Result from filtering the radargram with various directional Gaussian filters and taking the maximum response at each pixel.

The pixel values resulting from each Gaussian filter were compared, and the final image was created by taking the maximum value for each pixel across all filtered images. An example output from this approach is shown in Figure 5.

The motivation behind this approach was its ability to enhance any edge in the image regardless of orientation. This was appropriate for the bed detection in particular, as the edge orientation could vary drastically along the bed. However this method did not perform well, likely due to the nature of the noise present in these images. Because strong point reflectors produce reflection hyperbola over dozens of pixels, the directional Gaussian filters also enhanced the noise in the radargrams and resulted in a decreased successful identification rate. Another primary drawback to this method was the computational time required, as many large Gaussian filters had to be applied across the entire image. This resulted in the Gaussian filter approach taking almost 10 times as long as our other methods. A potential alternative to this implementation would be to use steerable filters, which would reduce computational time and potentially improve results [2].

2.1.4 Morphological tophat filter

As pre-processing for Dijkstra's algorithm-based layer tracing described in section 2.3.2, we applied the morphological tophat filter, which takes the morphological opening of the image using a circular structuring element and then subtracts the result from the original image. This filter attenuates non-layer pixels, thereby preventing these pixels from being selected in the Dijkstra's algorithm-based layer tracing. An example output from this filtering process is shown in Figure 6.

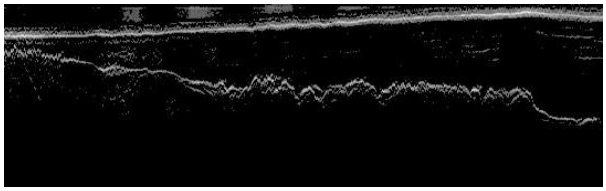

Figure 6. Output from the morphological tophat filtering used as input to Dijkstra's algorithm.

2.2. Seed point selection

We performed 1-d peak finding along each column of the edge enhanced image, particularly the wavelet transformed image shown in Figure 4. The identified peaks were filtered to remove subsidiary peaks having a prominence of less than 10% of the intensity of the maximum peak. A peak's "prominence" measures the peaks minimum rise above adjacent local minima. The remaining peaks were then sorted by intensity, with the strongest peak corresponding to the surface layer. Any peaks within a threshold number of vertical pixels from the surface layer were removed. The threshold 100 pixels worked well because this was the minimum distance between the surface layer and any other distinguishable layer through the radargrams. The strongest of the remaining peaks was selected as the bed layer. The seed points detected from the wavelet-transformed image are shown overlaid on the original radargram in Figure 8.

This approach worked well when the bed was near the surface. However, as the bed deepened, the signal-to-noise ratio of the bed diminished due to geometric spreading losses and englacial attenuation of the radar signal. Even though the wavelet transform preferentially enhances the wide bed signal over narrow englacial layers, strong englacial layers tended to have stronger responses than the bed when the bed dropped 1000 pixels (3000 m) below the surface, or when the bed was less reflective (e.g. due to increased roughness).

Following-peak detection, small gaps in the surface and bed were filled with a 5-point median filter. The median filter also removed outliers. The median filter was sufficient to remove virtually all outliers and gaps for the surface layer, but it was insufficient for removing outliers in the bed layer.

To further remove outliers, we performed morphological closing on a binary image with seed points represented as a 1 and all other points represented as a 0. This step removed all seed points that were not connected to at least four other seed points by edge or by vertex, which eliminated most spurious points that were not a part of the surface or the bed and improved the bed detection performance.

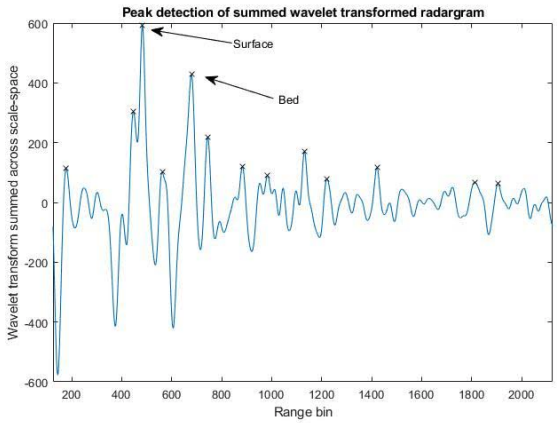

Figure 7. Peak detection along one column of the wavelet-transformed image. Detected peaks having a minimum height and prominence are marked in black.

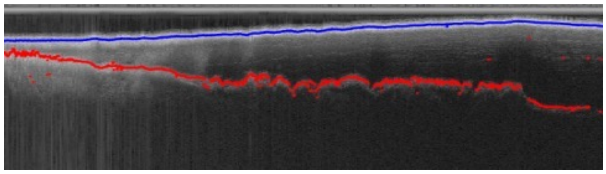

Figure 8. Seed points of surface and bed layers overlaid on original radargram.

2.3. Layer tracing

Using the seed points, the last stage in our pipeline traces the surface and bed layers to fill in columns without seed points and to ensure all picked points lie within a certain distance of their neighboring picked points. We applied two approaches including a local max search and Dijkstra's algorithm.

2.3.1 Local maximum search

The most successful approach we implemented for layer tracing was a local search for maximum intensity values in the wavelet-transformed image. To determine where to start the local maximum search, we performed region labeling on the seed points. The region with the greatest number of surface seed points (i.e. the region where the most surface seed points were connected by edge or by vertex) was taken to be the starting region for the surface tracing; similarly, the region with the greatest number of bed seed points was taken to be the starting region for the bed. From the end pixels in the starting regions, we searched in adjacent columns within a +7px/-7px vertical range for the maximum intensity value in the filtered radargram. The maximum intensity

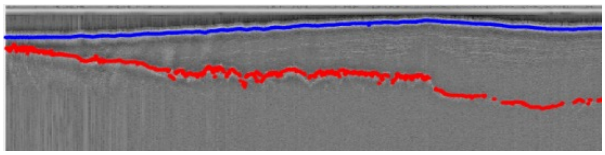

Figure 9. Layers traced by local adjacent maximum search.

value within this search range was appended to the initial region as a surface or bed point. This process was then repeated using the newly-chosen end points as the start values to define the search region. When the search encountered a seed point in a search column, it stopped its search for the maximum value in the search range and instead chose the seed point. This process, extended to all columns in the image, produced one surface and one bed index for each column. The layers we traced using this algorithm are shown in Figure 9.

2.3.2 Dijkstra's algorithm

We also tested Dijkstra's algorithm to trace between the seed points. Using regularly spaced seed points, we used the algorithm to find the shortest path between two seed points. By tracing outwards along the set of nodes whose shortest path from the starting seed point is known, eventually every pixel along the shortest path will be reached. The weights used to determine distance are a weighted sum of different metrics such as length of the edge, location of node in relation to start, and end seed points and intensity of node compared to neighboring nodes. In other words, the algorithm favors taking the geometrically shortest and brightest path. To improve performance, only intensity values $> 0.35*$maximum pixel intensity were allowed for tracing. However, this method did not perform as well as we expected. We believe this is because the bed layer often has jagged edges and quick changes of slope. Dijkstra's algorithm smoothed out this bumpy bed layer too much, resulting in a low success rate. The bed layer tracing from Dijkstra's algorithm is shown in Figure 10. It should also be noted that Dijkstra's algorithm stores a queue of all paths searched so far, resulting in significantly higher memory usage than other layer tracing algorithms we considered. Our implementation (porting C++ code into MATLAB) was constrained to processing about 10% of the image width at a time due memory limits. Although this particular limitation could be fixed with a pure C++ implementation, it doesn't fix the algorithm's inherently larger memory footprint.

3. Bed and surface identification results

To test the algorithm, we used radargrams obtained by the University of Texas at Austin and the British Antarc-

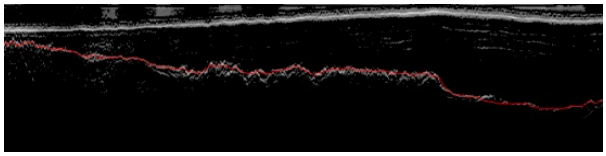

Figure 10. Bed layer as identified by Dijkstra's algorithm.

tic Survey during the 2004/2005 survey of West Antarcticas Amundsen Sea Embayment [3]. We tested on five focused radargrams, each of which surveyed about 270km in the azimuthal direction with a spacing of 17.5m. The image's vertical dimension corresponds to the range direction, with each pixel having a spacing of 3m. These radargrams were available in log-detected magnitude form (analogous to a grayscale image), and already had human-verified bed and surface picks identified against which we compared the output of our algorithm. In testing our pipeline, we tested only picks that had $>$10dB SNR, and did not include floating ice in the images.

We used successful surface and bed identification percentages as a performance metric. For each column, the identification of the surface and bed pick was declared a success if it lay within a threshold number of pixels from the reference, human-selected picks. Since the surface and bed layers have vertical widths of about 20px in flat regions, but the vertical width of the bed can approach 50px over a horizontal run of 10px, we used two different thresholds of 20px and 50px for all methods we investigated. The reference picks vary within a 10px range vertically, so we selected the 20px range as the smaller threshold within which our results effecitvely matched the reference picks. We used 50px as an upper threshold because existing processing tools within Dustin Schroeder's Radioglaciology research group are robust to pick errors of up to 50px.

It should be noted that the previous human-verified picks were chosen to identify the bed layer onset (leading edge of bed layer return). For purposes of characterizing basal properties based on radar return power, the pixel with the maximum intensity value in the layer is of most interest. This accounts for some of the differences between the existing labels and the picks produced by our automated method. To demonstrate the sensitivity of the success rate to the pixel threshold, Figure 11 plots the success rate against pixel threshold. The success rate is relatively insensitive to increasing the threshold above 10px for the surface and 50px for the bed.

4. Detecting internal layers

The seed selection described in section 2.1.2 has a useful extension for detecting internal layers. The peaks remaining after selecting the surface and bed are filtered to remove any peaks within a threshold vertical distance from the identified surface and bed (as identified by layer tracing in Section 2.3). The remaining peaks' intensities were fit to a log-normal distribution. When comparing the cumulative distribution functions (cdf) of the remainining peaks intensities versus the log-normal fit, it is apparent that there is a fat tail comprising about 30-40% of the peaks which are more frequent than would be predicted by the log-normal fit distribution. Thus, we set an intensity threshold at the point above the median where the empirical cdf exceeds the log-normal cdf, as suggested by [5]. When the peaks with intensities above this threshold are plotted on the original radargram as in Figure 12 we see they correspond well to internal layers.

[5] describes a local Hough transform-based layer tracing procedure for filling in gaps in the internal layers. Although we considered implementing this procedure, we ultimately focused on improving bed layer tracing because it is more applicable to the Stanford Radioglaciology group's current research.

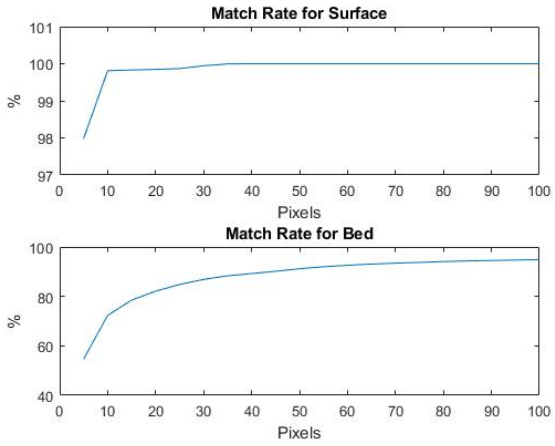

Figure 11. Success rate plotted against pixel threshold.

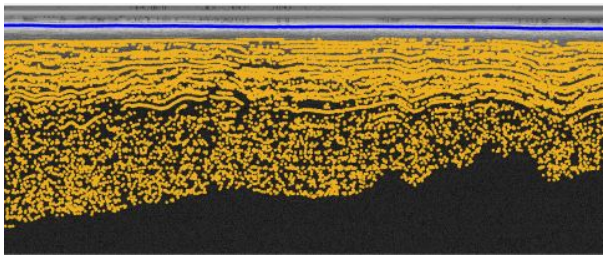

Figure 12. Internal layers identified by filtering non-surface and non-bed peaks are plotted in yellow. Surface pick plotted in blue.

Method	Surface Pik within 20 pixels	Surface Pik within 50 pixels	Bed Pik within 20 pixels	Bed Pik within 50 pixels	Processing time per column
(A) Peak detection on radargram	99.9%	100.0%	40.2%	57.5%	0.03ms
(B) Local adjacent max tracing on Gaussian filtered radargram	99.31%	100.0%	47.57%	59.1%	36.7ms
(C) Peak detection on wavelet tx'd radargram	99.8%	100.0%	82.1%	91.2%	3ms
(D) Dijkstra's algorithm-based tracing	-	-	18.3%	53.0%	3.6ms
(E) Local adjacent max tracing on output of (C)	99.9%	100.0%	83.73%	93.69%	3.6ms

Table 1. Results.

5. Future Work

5.1. SAR processing techniques to remove internal layers

Recent work by Davide Castelleti, Dustin Schroeder, and others (in prep) approaches focused synthetic aperture radar processing as an optimization problem. Standard focused SAR processing assumes that layers are either flat specular reflectors or isotropic reflectors. However, most internal layers have a gradually varying slope slightly deviating from the horizontal assumption. Given a layer's slope, phase differences due to the slope can be corrected, increasing the horizontal distance over which radar returns can be coherently summed, thereby improving the SNR of the layer. Castelleti et al. use optimization techniques to find the slope of each layer by maximizing the layer power.

This focusing technique can be hijacked to improve detection of the bed. Unlike internal layers (which are mostly specular reflectors), the bed is an isotropic reflector. In other words, the bed reflection power is insensitive to a phase correction based on bed slope; internal layer power is sensitive to such a slope-based correction. Thus, focusing the radargram based on a deliberately incorrect layer slope (e.g., between 45 and 90 degrees from horizontal) would drastically reduce internal layer power compared to bed layer power.

The techniques described herein sometimes confuse the bed layer with near-surface internal layers, particularly when the bed layer has low SNR. This confusion would be prevented if the input radargram had significantly diminished internal layers. Thus, applying a modified version of the SAR processing technique of Castelleti et al. would produce a radargram image that would improve our image processing performance.

5.2. Machine-learning informed layer tracing

The most successful layer tracing technique we used was selecting the local adjacent maximum. This approach works well for filling in small gaps between seed points as long as the underlying image (typically an edge detected and sharpened image as described in Section 2.1.2) has a bed layer with sufficient power. However, the bed layer experiences significant gaps where the power drops significantly over a horizontal stretch of 10-20 pixels, followed by a return of a strong bed signal, often displaced up or down by 25-50 pixels. These gaps in the bed signature tend to stump the local max tracing we described.

A more sophisticated layer tracing would consider pixels over a local region, including both traced pixels behind and untraced pixels ahead. The vertical and horizontal dimensions of the region are difficult to set. When the bed is in a shallow region, a narrow vertical window is advantageous because there are likely adjacent internal layers that could cause confusion. When the bed is deeper, a taller vertical window would be more advantageous. Other factors affecting the vertical window size include the slope of the already traced layer. Attempting to identify a useful set of search

region dimensions and a set of thresholds for using different search region dimensions is a difficult, error-prone task that would be prone to overfitting the dataset.

Instead, it would be better to use supervised machine learning techniques to adaptively determine the search region dimensions based on local features. Such features could include (i) the vertical displacements and (ii) powers of preceding traced points; (iii) the number of seed points identified in un-traced columns; (iv) the slope of preceding traced points; and (v) the peak width and peak prominence of traced points and un-traced seed points. The machine learning algorithm could attempt to maximize the likelihood that the search region contains the "correct" bed pik (using the reference piks as training data) by varying the search window. This search window would then be used to pick the bed based on the max within the region.

Alternatively, the machine learning algorithm could attempt to directly pick the bed based on (i) any of the preceding features, (ii) the powers of candidate pixels, (iii) the edge-detected powers of candidate pixels, or (iv) a measurement of smoothness or continuity among selected pixels. This might be implemented as supervised learning, a neural network, or an optimization function (that maximizes an objective function maximizing traced power and minimizing discontinuities).

References

[1] G. J. Freeman, A. C. Bovik, and J. W. Holt. Automated detection of near surface martian ice layers in orbital radar data. In *2010 IEEE Southwest Symposium on Image Analysis Interpretation (SSIAI)*, pages 117–120, May 2010.

[2] W. T. Freeman and E. H. Adelson. The design and use of steerable filters. *IEEE Transactions on Pattern Analysis and Machine Intelligence*, 13(9):891–906, Sep 1991.

[3] J. W. Holt, D. D. Blankenship, D. L. Morse, D. A. Young, M. E. Peters, S. D. Kempf, T. G. Richter, D. G. Vaughan, and H. F. J. Corr. New boundary conditions for the west antarctic ice sheet: Subglacial topography of the thwaites and smith glacier catchments. *Geophysical Research Letters*, 33(9):n/a–n/a, 2006. L09502.

[4] C. Panton. Automated mapping of local layer slope and tracing of internal layers in radio echograms. *Annals of Glaciology*, 55(67):7177, 2014.

[5] S. Xiong, J.-P. Muller, and R. C. Carretero. A new method for automatically tracing englacial layers from mcords data in nw greenland. *Remote Sensing*, 10(1), 2018.

Final Output for Radargram X69a

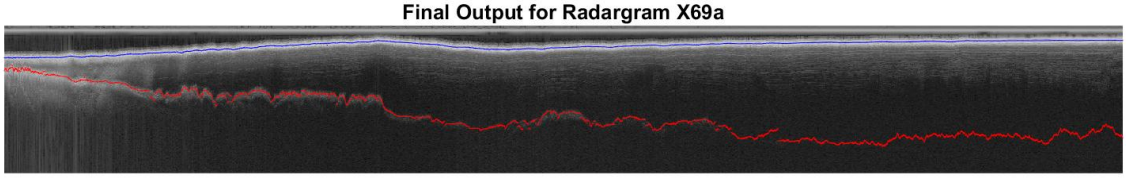

Final Output for Radargram X73a

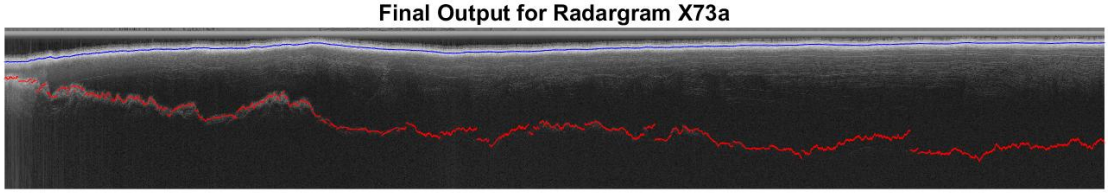

Final Output for Radargram X75a

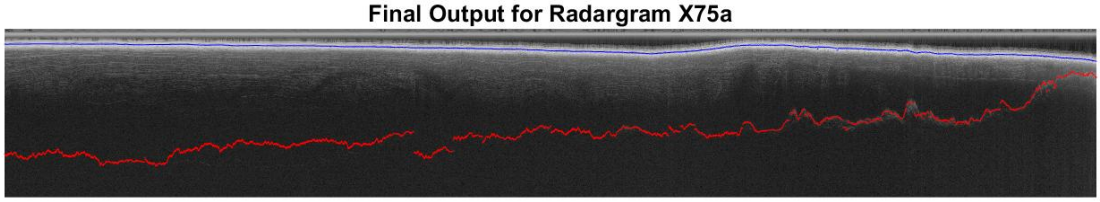

Final Output for Radargram X79a

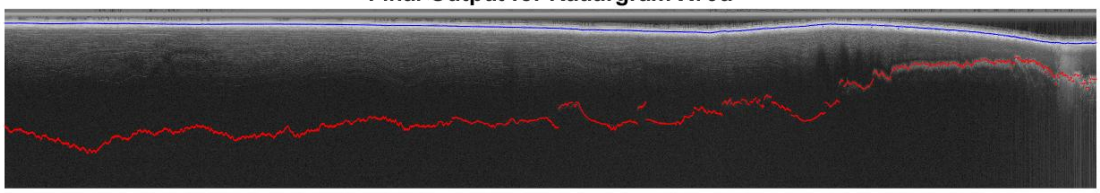

Final Output for Radargram X81a

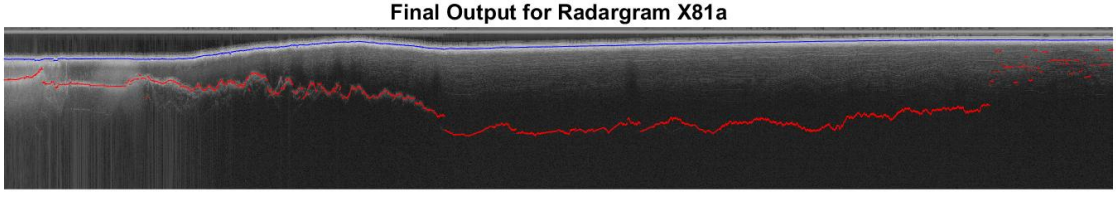

Appendix: Division of Labor

Andrew Hilger: implemented and optimized Ricker wavelet edge enhancement; developed seed point detection following Ricker wavelet; implemented algorithms for selecting seedpoints for englacial layers; organized dataset and created testbench; future work section.

Sarah Hooper: implemented the rotating Gaussian filter edge enhancement method; tested basic edge detectors (central difference, Sobel, Roberts) for edge enhancement stage; developed local adjacent maximum layer tracing.

Cedric Yue Sik Kin: tested Prewitt edge detection approach to layer identification; wrote code to use morphological tophat filter for edge enhancement; implemented Dijkstra's algorithm.

All: created poster; wrote paper sections corresponding to above division of labor.